XV International Conference on Computational Plasticity. Fundamentals and Applications
COMPLAS 2019
E. Oñate, D.R.J. Owen, D. Peric, M. Chiumenti & Eduardo de Souza Neto (Eds)

ANALYSIS OF DAMAGE AND FRACTURE MECHANISMS IN DUCTILE METALS UNDER NON-PROPORTIONAL LOADING PATHS

MICHAEL BRÜNIG*, STEFFEN GERKE* AND MORITZ ZISTL*

* Institute for Engineering Mechanics and Structural Analysis
Bundeswehr University Munich
85577 Neubiberg, Germany
e-mail: michael.bruenig@unibw.de, web page: http://www.unibw.de/mechanik-und-statik

Key words: Damage and fracture, ductile metals, non-proportional loading, experiments, numerical simulations

Abstract. The paper discusses biaxial experiments and corresponding numerical simulations to analyze the effect of non-proportional loading paths on damage and fracture behavior of ductile metals. Newly developed specimens are taken from thin metal sheets and are tested under different biaxial loading conditions covering a wide range of stress states. In this context, an anisotropic continuum damage model is presented based on yield and damage conditions as well as on evolution laws for plastic and damage strain rates. Different branches of the damage criteria are taken into account corresponding to various damage and failure processes on the micro-level depending on stress triaxiality and Lode parameter. Experiments with biaxially loaded specimens have been performed. Results for proportional and corresponding non-proportional loading histories are discussed. During the experiments strain fields in critical regions of the specimens are analyzed by digital image correlation (DIC) technique while the fracture surfaces are examined by scanning electron microscopy (SEM). Numerical simulations of the experiments have been performed and numerical results are compared with experimental data. In addition, based on the numerical analyses stress distributions in critical parts of specimens are detected. The results demonstrate the efficiency of the new specimen's geometries covering a wide range of stress states in the shear/tension and shear/compression regime as well as the effect of loading history on damage and fracture behavior in ductile metal sheets.

1 INTRODUCTION

Products of modern metal forming processes have to fulfill requirements of the customers. These are, for example, demands to enforce safety of structural elements or to develop lightweight structures leading to cost reduction or to improvements in energy consumption. These environmental, economic and safety aspects lead to increased inquiries for high quality metals like aluminum alloys or high strength and advanced high

strength steels. On the other hand, numerical studies to optimize metal forming processes have received remarkable attention during the last decades. Thus, highly predictive and practically applicable constitutive models as well as corresponding efficient and accurate numerical algorithms have to be developed to investigate damage and fracture processes on the micro-scale causing macro-defects and fracture in materials and structural elements. Since many industrial processes like forging and rolling undergo non-proportional loading scenarios the analysis of damage and fracture mechanisms caused by non-proportional loading paths is of special interest.

Nowadays it is well known that the stress state acting in a material point affects the damage and failure processes on the micro-scale. For example, formation and growth of nearly spherical micro-voids occur under hydrostatic stress whereas micro-shear-cracks are caused by deviatoric stress states. To examine and to understand these different stress-state-dependent damage and failure mechanisms and their interactions detailed experimental and numerical analyses have to be performed on both the micro- and the macro-scale allowing development of accurate and realistic phenomenological material theories. These constitutive models can be used to quantify damage at different stages of the loading processes as well as to judge the quality of metal forming processes.

In the literature various experiments with different specimens have been proposed to study the effect of stress state on damage and fracture mechanisms as well as their influence on the inelastic deformation and macroscopic failure behavior of ductile metals. For example, in the analysis of sheet metal behavior under positive stress triaxialities enforcement of uniaxial tension tests with unnotched and differently notched flat specimens has been proposed in combination with corresponding numerical simulations [1, 2, 3, 4, 5]. On the other hand, specimens with new geometries have been presented and tested under uniaxial loading conditions to investigate their deformation, damage and fracture behavior under nearly zero stress triaxialities leading to micro-shear-crack processes on the micro-level in their critical parts [1, 2, 4, 5, 6]. In addition, butterfly specimens have been developed to study the effect of different stress states on failure behavior in ductile materials. These specimens are loaded in different directions in a special test equipment leading to combined tensile, shear and compressive stress states [3, 6]. Alternatively, experiments with biaxially loaded flat cruciform specimens have been developed [7]. Further biaxial experiments with newly developed specimens have been presented [8, 9, 10]. Corresponding numerical calculations have been performed to examine the stress states in critical specimens regions to analyze stress-state-dependent damage and fracture processes in thin ductile metal sheets. In addition, first results of experiments with biaxially loaded specimens undergoing non-proportional loading paths have been discussed [11]. They show remarkable influence of the non-proportional loading history on damage and fracture mechanisms.

From theoretical point of view anisotropic continuum damage models seem to be most qualified to predict inelastic deformations as well as stress-state-dependent damage and fracture behavior of ductile sheet metals. On the other hand, their practical use may be limited by large number of constitutive parameters and problems in their identification. Thus, in the present paper an efficient phenomenological anisotropic continuum damage

model is discussed. Results of experiments with biaxially loaded specimens under proportional and corresponding non-proportional loading conditions are shown. Evolution of strain fields are monitored by digital image correlation (DIC) technique and fracture surfaces are visualized by scanning electron microscopy (SEM). Corresponding numerical simulations of the experiments are used to reveal the stress states in critical regions of the specimens allowing explanation of the failure mechanisms shown on the fracture surfaces.

2 CONTINUUM DAMAGE MODEL

The continuum damage model presented in [12, 14] is briefly discussed. With this phenomenological approach inelastic deformations as well as anisotropic evolution of damage in ductile metals are numerically predicted. Stress-state-dependent damage and fracture processes on the micro-scale are accompanied by the formation of macroscopic damage strains. The thermodynamically consistent continuum framework takes into account damaged as well as corresponding fictitious undamaged configurations. The kinematic approach is based on the introduction of elastic, plastic and damage strain rate tensors. Elastic constitutive equations are based on free energy functions formulated in the damaged and undamaged configurations, respectively, and are able to simulate the deteriorating effect of damage on elastic material properties. In addition, considering the undamaged configurations isotropic plastic behavior is governed by a yield criterion and a non-associated flow rule. In a similar way, considering the damaged configurations anisotropic damage behavior is modeled by a damage condition and a damage rule both depending on the stress triaxiality and the Lode parameter to take into account the effect of stress state on damage and fracture behavior.

In particular, isotropic plastic behavior of the investigated aluminum alloy AlSiMgMn (EN AW 6082-T6) is governed by the yield criterion

$$f^{pl} = a\bar{I}_1 + \sqrt{\bar{J}_2} - c = 0 \tag{1}$$

where the first and second invariants, $\bar{I}_1$ and $\bar{J}_2$ of the effective Kirchhoff stress tensor [12] have been used. The plastic hardening behavior of the analyzed aluminum alloy is characterized by the power law

$$c = c_0 \left(\frac{H_0\,\gamma}{n\,c_0} + 1 \right)^n \tag{2}$$

taking into account the initial yield stress $c_0 = 163.5$ MPa, the initial hardening modulus $H_0 = 850$ MPa as well as the hardening exponent $n = 0.182$, and γ represents the equivalent plastic strain measure [12].

In addition, onset and continuation of damage is determined by a damage surface formulated in stress space [12, 13]. In this context, the damage criterion

$$f^{da} = \alpha I_1 + \beta\sqrt{J_2} - \sigma = 0 \tag{3}$$

is expressed in terms of the first and second deviatoric stress invariants I_1 and J_2 of the Kirchhoff stress tensor. In Eq. (3), the equivalent damage stress measure

$$\sigma = \sigma_0 - H_1\,\mu^2 \tag{4}$$

characterizes deterioration of material properties caused by micro-defect propagation [15] with the initial equivalent stress $\sigma_0 = 250$ MPa and the modulus $H_1 = 400$ MPa where μ denotes the equivalent damage strain measure. In Eq. (3) the variables α and β represent damage mode parameters associated with the different stress-state-dependent damage mechanisms acting on the micro-level: void-growth-dominated modes for large positive stress triaxialities, shear modes for negative stress triaxialities and mixed modes (simultaneous growth of voids and formation of micro-shear-cracks) for moderate positive and nearly zero stress triaxialities. In the present continuum damage model, the effect of the Lode parameter is also taken into account because it has been shown that its influence on the formation of the micro-structural processes can be remarkable especially in moderate positive and negative stress triaxiality regions [14]. Hence, the damage mode parameters α and β in the damage criterion (3) depend on the stress intensity $\sigma_{eq} = \sqrt{3J_2}$ (von Mises equivalent stress), the stress triaxiality

$$\eta = \frac{\sigma_m}{\sigma_{eq}} = \frac{I_1}{3\sqrt{3J_2}} \tag{5}$$

defined as the ratio of the mean stress $\sigma_m = I_1/3$ and the von Mises equivalent stress σ_{eq} as well as on the Lode parameter

$$\omega = \frac{2T_2 - T_1 - T_3}{T_1 - T_3} \quad \text{with } T_1 \geq T_2 \geq T_3 \tag{6}$$

expressed in terms of the principal Kirchhoff stress components T_1, T_2 and T_3.

The dependence of α and β on stress state has been studied in detail for aluminum alloys. Numerical analyses on the micro-scale have been performed [14] considering the deformation and failure behavior of void-containing unit cells. Use of simplified functions has been discussed in [9] for practical applications still allowing accurate phenomenological modeling of inelastic deformations as well as of damage and failure behavior in comparison with experiments with biaxially loaded specimens. With these functions the parameters α and β are related to different stress-state-dependent damage and fracture mechanisms acting on the micro-level.

Based on these investigations [9, 14], the parameter α is given by

$$\alpha(\eta) = \begin{cases} 0.0 \;\text{ for }\; \eta \leq 0 \\ 0.33 \;\text{ for }\; \eta > 0 \end{cases} \tag{7}$$

whereas the parameter β is taken to be the non-negative function

$$\beta(\eta, \omega) = -1.28\,\eta + 0.85 - 0.017\,\omega^3 - 0.065\,\omega^2 - 0.078\,\omega \;\geq\; 0\;. \tag{8}$$

Furthermore, the damage strain rate tensor is given by the damage rule

$$\dot{\mathbf{H}}^{da} = \dot{\mu}\left(\bar{\alpha}\,\frac{1}{\sqrt{3}}\,\mathbf{1} + \bar{\beta}\,\mathbf{N}\right) \tag{9}$$

where $\dot{\mu}$ denotes a non-negative scalar-valued factor. In Eq. (9) the stress related deviatoric tensor $\mathbf{N} = \frac{1}{2\sqrt{J_2}}\,\mathrm{dev}\tilde{\mathbf{T}}$ has been used and $\dot{\mu}$ is in the present continuum damage model the equivalent damage strain rate measure quantifying the amount of increase in irreversible damage. The parameters $\bar{\alpha}$ and $\bar{\beta}$ are kinematic variables representing the portion of volumetric and isochoric damage-induced deformations. These parameters also correspond to different damage and fracture mechanisms on the micro-level and, similar to the parameters in the damage criterion (3), they have been identified by numerical analyses with micro-defect-containing representative volume elements undergoing different three-dimensional loading scenarios [14] as well as on comparison of experimental data and results of numerical simulations of experiments with uniaxially and biaxially loaded specimens [9].

In particular, the stress-state-dependence of the parameter $\bar{\alpha}$ related to the amount of volumetric damage strain rates caused by volume changes of micro-defects is written in the form

$$\bar{\alpha}(\eta) = \begin{cases} 0 \;\text{ for }\; \eta \leq 0 \\ 0.5714\,\eta \;\text{ for }\; 0 < \eta \leq 1.75 \\ 1 \;\text{ for }\; \eta > 1.75 \end{cases} . \tag{10}$$

In additon, the stress-state-dependence of the parameter $\bar{\beta}$ modeling the amount of anisotropic isochoric damage strain rates caused by formation of micro-shear-cracks is given by

$$\bar{\beta}(\eta,\, \omega) = \bar{\beta}_0(\eta) + (-0.0252 + 0.0378\,\eta)\; \bar{\beta}_\omega(\omega) \tag{11}$$

with

$$\bar{\beta}_0(\eta) = \begin{cases} 0.87 \;\text{ for }\; \eta \leq \frac{1}{3} \\ 0.979 - 0.326\,\eta \;\text{ for }\; \frac{1}{3} < \eta \leq 3 \\ 0 \;\text{ for }\; \eta > 3 \end{cases} \tag{12}$$

and

$$\bar{\beta}_\omega(\omega) = \begin{cases} 1 - \omega^2 \;\text{ for }\; \eta \leq \frac{2}{3} \\ 0 \;\text{ for }\; \eta > \frac{2}{3} \end{cases} . \tag{13}$$

It can be clearly seen that the macroscopic damage rule (9) takes into account a volumetric part (first term in Eq. (9)) corresponding to isotropic growth of voids on the micro-level as well as a deviatoric part (second term in Eq. (9)) associated with the anisotropic development of micro-shear-cracks, respectively. Therefore, the basic damage mechanisms discussed above (growth of isotropic voids and evolution of micro-shear-cracks) acting on the micro-scale are involved in the macroscopic damage rule (9) of the phenomenological continuum model.

3 EXPERIMENTS AND NUMERICAL SIMULATIONS

An experimental program has been developed to analyze stress-state-dependent behavior in biaxially loaded specimens [10]. The experiments are performed using the biaxial test machine type LFM-BIAX 20 kN. The specimens are biaxially loaded by four electromechanically and individually driven cylinders and are clamped in the four heads of the

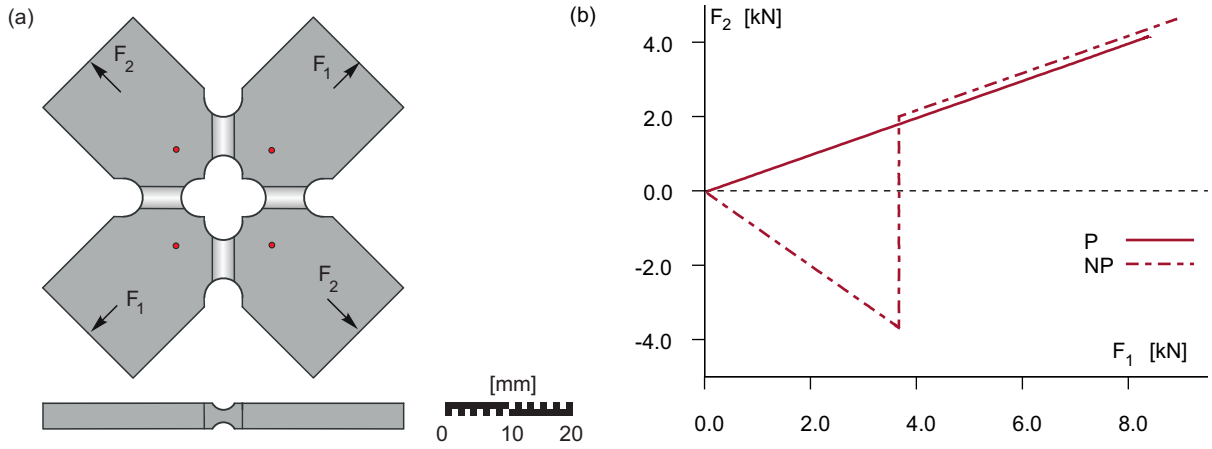

Figure 1: Loading paths

cylinders. Further tests with the X0-specimen to investigate inelastic deformations as well as damage and fracture processes on the micro-level for different proportional and non-proportional loading histories have been performed [11]. The specimens are manufactured from ductile metal sheets with 4 mm thickness and the central part of the geometry of the X0-specimen as well as the acting forces are shown in Fig. 1(a). There are four notched regions with minimum thickness of 2 mm where localization of inelastic strains and damage are expected to occur. In addition to former tests [11] in the present paper the behavior of the X0-specimen for the load ratio $F_1/F_2 = 1/0.5$ is discussed where experimental data are compared with results from corresponding numerical simulations. Proportional (P) and non-proportional (NP) loading paths are taken into account (see Fig. 1(b)) and the influence of the loading history on damage and fracture processes is studied in detail. In the non-proportional case first loading is by the load ratio $F_1/F_2 = 1/-1$ and at the stage $F_1 = -F_2 = 3.8$ kN additional tensile loading by F_2 occurs. When this loading path reaches that one of the proportional case a final proportional part follows until final fracture of the specimen occurs. In these tests with the load ratio $F_1/F_2 = 1/0.5$ the final loads for the non-proportional loading history are about 10% larger than the final loads of the proportional case. Thus, the loading path has an influence on the fracture force.

Corresponding numerical analysis of the specimen's behavior during the biaxial tests are performed to get data of the stress fields acting in the specimens allowing prediction of damage and failure modes. The simulations are carried out using the finite element program ANSYS enhanced by a user-defined material subroutine based on the presented continuum damage model. The X0-specimen is discretized by eight-node-elements of type Solid185.

Figure 2 shows load-displacement curves of experiments and numerical simulations for loads and displacements in axis 1 (a1) and axis 2 (a2) where Δu_{ref} represents the displacements in axis 1 and axis 2, respectively, between the two opposite red points shown in Fig. 1(a). Under the proportional loading case (Fig. 2(a)) the load F_1 in axis 1 (a1) increases and at $F_1 = 6.2$ kN onset of plastic yielding can be seen. Further increase

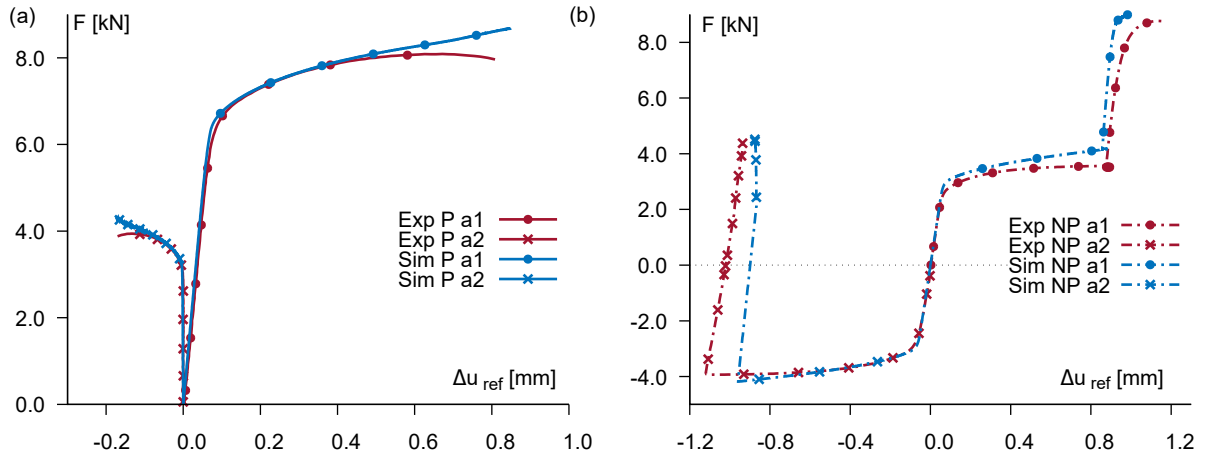

Figure 2: Load-displacement-curves: (a) P, (b) NP

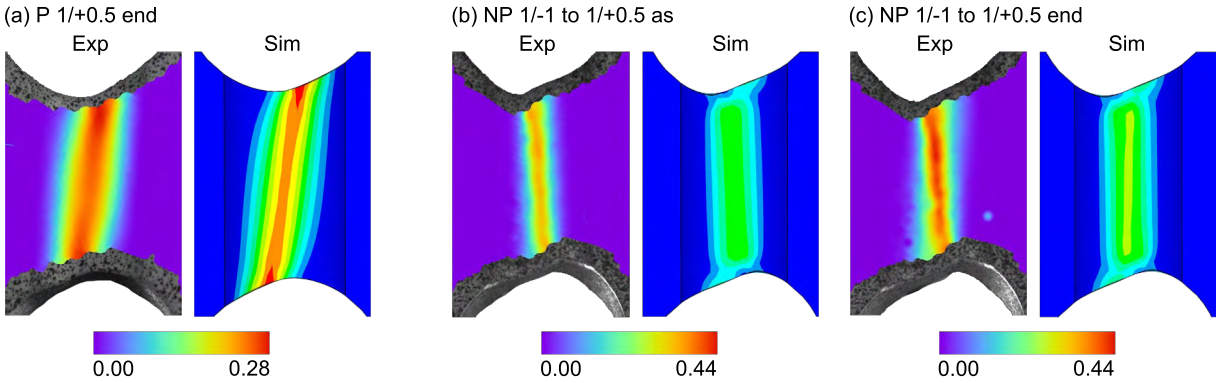

Figure 3: Strain fields (first principal strain) in the notched region

in load is measured and the specimen fails at $\Delta u_{ref1} = 0.8$ mm. In axis 2 (a2) at the load level $F_2 = 3.1$ kN plastic yielding begins and the specimen fails at $\Delta u_{ref2} = -0.2$ mm. The load-displacement curves of the experiments (Exp) and of the numerical simulation (Sim) agree well, only at the end of the test small differences can be seen. In addition, during the non-proportional loading path (Fig. 2(b)) the load in axis 1 (a1) increases up to $F_1 = 2.4$ kN where onset of plastic yielding can be observed. During further increase in load displacements increase up to $\Delta u_{ref1} = 0.9$ mm. Then, load F_2 increases whereas F_1 remains constant and during the final proportional loading step the load F_1 also increases up to final fracture. At this point, the displacement reaches $\Delta u_{ref1} = 1.1$ mm which is remarkably larger compared to the displacement after the proportional loading history. In axis 2 (a2) in the first loading step the displacement reaches $\Delta u_{ref2} = -1.1$ mm and at failure $\Delta u_{ref2} = -0.9$ mm is measured which again is remarkably larger than the final displacement in axis 2 after the proportional loading path. Also in the non-proportional case, the numerical results agree well with the experimental ones.

During the tests with the X0-specimens strain fields are monitored by digital image correlation (DIC) technique. Distributions of the first principal strain in one notched part

of the specimen taken from the experiments (Exp) and based on the numerical simulations (Sim) are shown in Fig. 3. In the tests with proportional loading paths (a) a widespread band of strains with maxima of about 28% and slight right-to-left-orientation can be seen and results of the experiments agree very well with those predicted by the corresponding numerical simulation concerning maxima and orientation of the localized strain field as well as the final shape of the notched region of the X0-specimen. During the tests with the non-proportional loading path after the first load step before axis switch (as) of the loads (Fig. 3(b)) a very small localized band of the first principal strain with maxima of about 35% occurs. Size and orientation of the small band of strains as well as the shape of the notched part of the specimen are well predicted by the numerical simulation whereas the maxima of the first principal strain are only about 23%. In addition, Fig. 3(c) shows the distribution of the first principal strain at the end of the non-proportional test (end). A small localized band of strains with maxima of 44% can be seen with slight left-to-right-orientation. A similar band of localized strains is predicted by the numerical simulation but the maxima are only 26%. The final shape of the notched part of the specimen at the end of the non-proportional test is well predicted. Analysis of the first principal strain fields caused by the proportional and the considered non-proportional loading paths show differences concerning the width and the size as well as the orientation of the localized bands as well as the final shape of the notched region.

Furthermore, distribution of the stress triaxiality η (Eq. (5)) and of the Lode parameter ω (Eq. (6)) predicted by the numerical simulations of the experiments are shown in Fig. 4. In particular, at the end of the proportional loading path (Fig. 4(a)) the distribution of the stress triaxiality in the cross section (C) is nearly homogeneous with maxima $\eta = 0.6$ in the central part. In the longitudinal section (L) of the notched part of the X0-specimen a widespread band of moderate triaxialities $\eta \geq 0.4$ with larger values in butterfly-shaped distribution in the central part with maxima $\eta = 0.6$ occurs. On the surface of the notch (S) the stress triaxialities are smaller with nearly homogeneous distribution. In addition, the Lode parameter shows in the notched region nearly homogeneous distribution with values up to $\omega = -1.0$ which is typical for tension-dominated stress states. On the other hand, after the first step of the non-proportional loading path NP(1) before axis switch (as) of the loads (Fig. 4(b)) the stress triaxiality η in the cross section (C) of the center of the notch is homogeneously distributed with $\eta = 0.0$ and a large region with this value can also be seen in the longitudinal section (L) and the surface of the notch (S). In addition, at this loading stage the corresponding Lode parameter ω is also homogeneously distributed in the cross section (C) with $\omega = 0.0$ and large regions of this value are also visible in the longitudinal section (L) and on the boundary (V), whereas in the center of the boundary slightly higher Lode parameters up to $\omega = 0.3$ can be seen. These stress fields are typical for shear-dominated stress states. Different stress parameters are numerically predicted at the end of the non-proportional loading scenario (NP(12)) shown in Fig. 4(c). Homogeneous field of the stress triaxiality with $\eta = 0.3$ is obtained in the notch and the corresponding Lode parameter is about $\omega = -1.0$. The numerically predicted distributions of the stress triaxiality and of the Lode parameter at the end of the proportional and the non-proportional loading paths are very similar and,

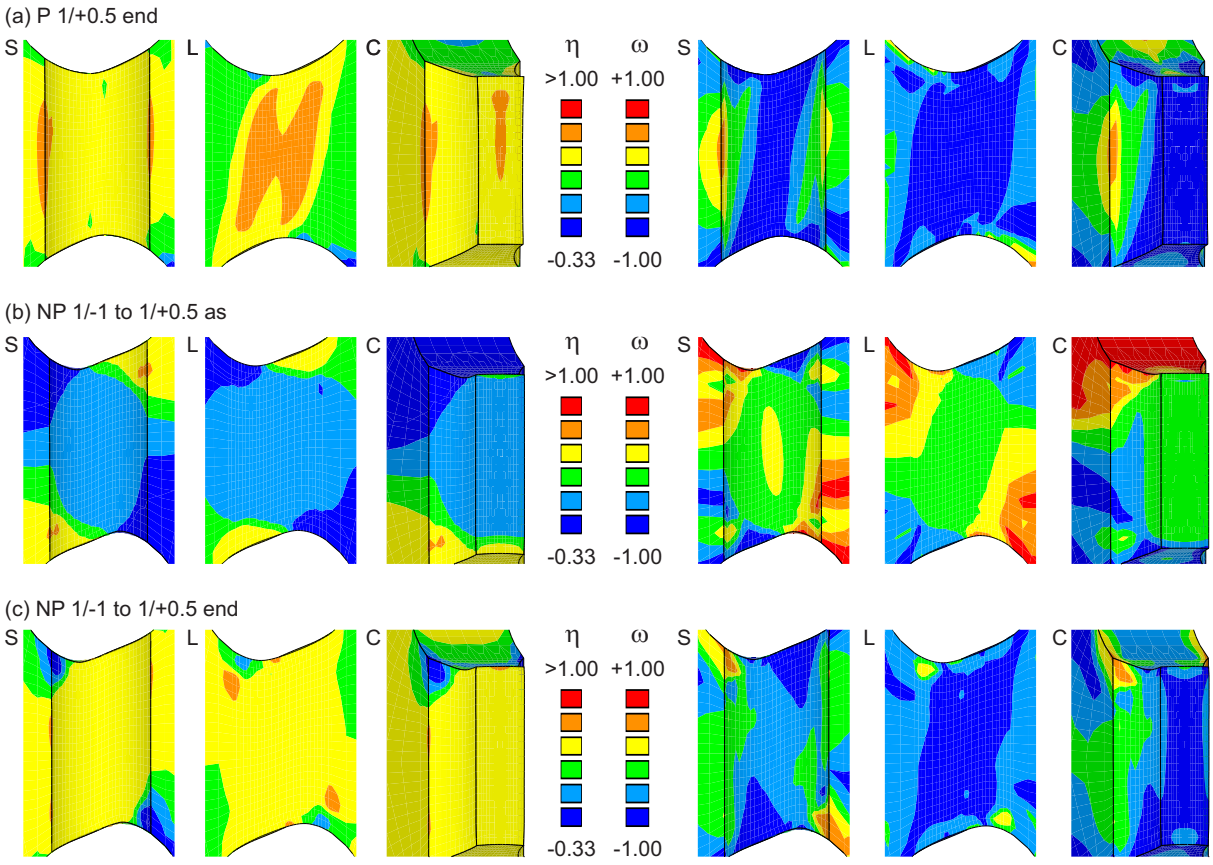

Figure 4: Stress triaxiality η and Lode parameter ω: (a) P, (b) NP (1), (c) NP (12); S = surface, L = longitudinal section, C = cross section

thus, nearly unaffected by the loading history.

Moreover, fracture lines are shown in Fig. 5. After the proportional loading scenario (Fig. 5(a)) nearly straight fracture lines occur with small angle with respect to the vertical line. After non-proportional loading (Fig. 5(b)) S-shaped fracture lines can be seen with vertical orientation. Thus, different fracture lines occur after the two investigated, different loading histories.

In addition, fracture behavior is analyzed in more detail by images of the fracture surfaces taken from scanning electron microscopy (Fig. 6). After the proportional loading path (Fig. 6(a)) remarkable formation of micro-voids can be seen which are slightly sheared. This failure behavior on the micro-level corresponds very well to the stress states shown in Fig. 4(a) with remarkable tensile stresses superimposed by small shear stresses in the notched regions. On the other hand, after the non-proportional loading history micro-shear-cracks with only very small voids are visible. During the first loading step with the load ratio $F_1/F_2 = 1/-1$ (NP(1)) shear behavior is predominant in the notched sections of the X0-specimen leading to formation of micro-shear-cracks. The subsequent increase in load F_2 and the later proportional loading step (NP(12)) lead to additional growth of few very small voids. Thus, different fracture modes are caused by

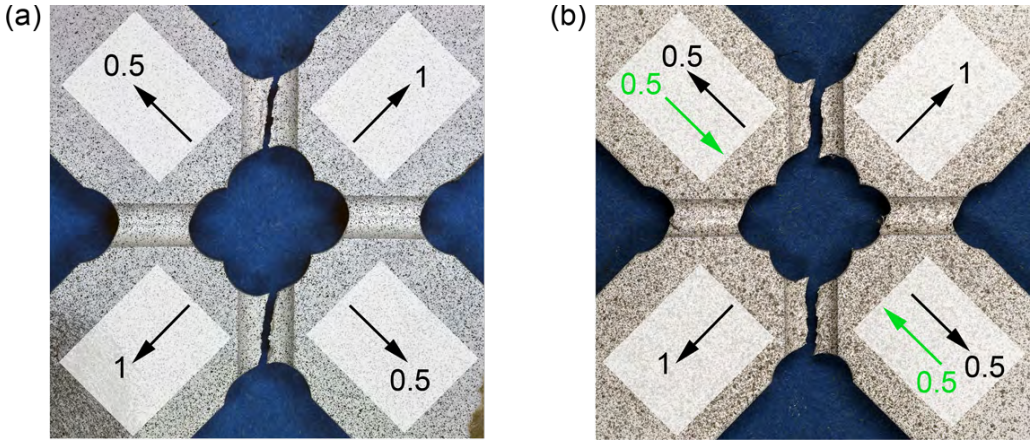

Figure 5: Fracture: (a) P, (b) NP

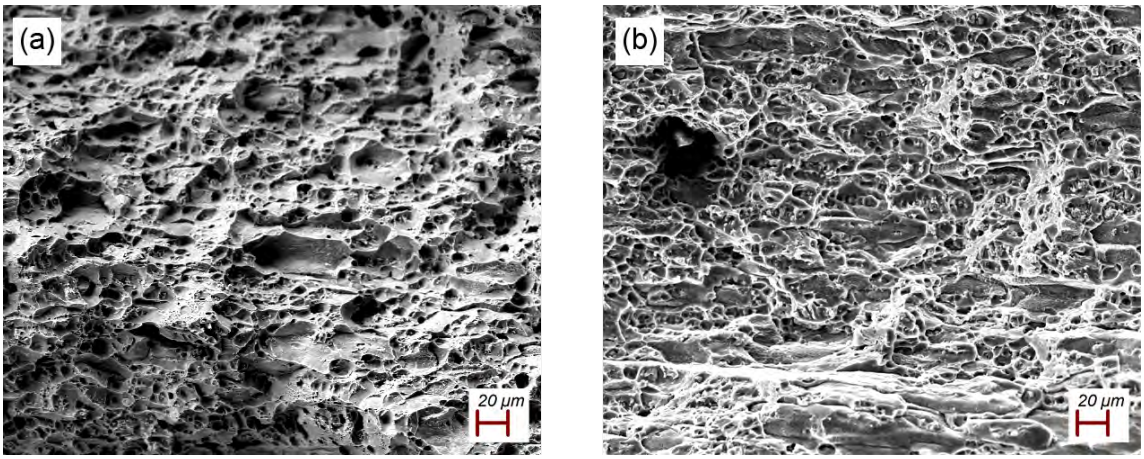

Figure 6: SEM picture of the fracture surface: (a) P, (b) NP

different loading scenarios.

4 CONCLUSIONS

A continuum damage model taking into account stress-state-dependent damage condition and damage rule has been discussed. The phenomenological approach has been validated by biaxial experiments with the X0-specimen with special focus on the effect of proportional and non-proportional loading histories as well as of different stress states on inelastic deformation as well as on damage and fracture behavior of ductile metals. Current strain fields in critical parts of the specimen have been monitored during the experiments by digital image correlation. After the tests fracture surfaces have been analyzed by scanning electron microscopy and showed remarkable differences depending on the loading histories. In addition, numerical simulations of the experiments have been performed. Numerically predicted load-displacement curves and distributions of principal strain fields as well as shapes of the deformed notched parts of the X0-specimen show

good agreement with experimental ones. Examination of numerically obtained stress fields are used to predict evolution of damage and fracture processes on the micro-scale which can be justified by scanning electron microscopy of the fracture surfaces. Therefore, the continuum damage model can be used to analyze and to optimize sheet metal forming processes with complex loading scenarios. Biaxial experiments with the X0-specimen are recommended to investigate stress-state-dependent damage and fracture processes in thin metal sheets.

Acknowledgement
The project has been funded by the Deutsche Forschungsgemeinschaft (DFG, German Research Foundation) – project number 322157331, this financial support is gratefully acknowledged. The SEM images of the fracture surfaces presented in this paper were performed at the Institut für Werkstoffe im Bauwesen, Bundeswehr University Munich and the support of Wolfgang Saur is gratefully acknowledged.

REFERENCES

[1] Bai, Y. and Wierzbicki, T. On the fracture locus in the equivalent strain and stress triaxiality space. *Int. J. Mech. Sci.* (2004) **46**:81-98.

[2] Gao, X., Zhang, G. and Roe, C. A study on the effect of the stress state on ductile fracture. *Int. J. Damage Mech.* (2010) **19**:75-94.

[3] Dunand, M. and Mohr, D. On the predictive capabilities of the shear modified Gurson and the modified Mohr-Coulomb fracture models over a wide range of stress triaxialities and Lode angles. *J.Mech. Phys. Sol.* (2011) **59**:1374-1394

[4] Brünig, M., Chyra, O., Albrecht, D., Driemeier, L. and Alves, M. A ductile damage criterion at various stress triaxilities. *Int. J. Plast.* (2008) **24**:1731-1755.

[5] Driemeier, L., Brünig, M., Micheli, G. and Alves, M. Experiments on stress-triaxiality dependence of material behavior of aluminum alloys. *Mech. Mat.* (2010) **42**:207-217.

[6] Bai, Y. and Wierzbicki, T. A new model of metal plasticity and fracture with pressure and Lode dependence. *Int. J. Plast.* (2008) **24**:1071-1096.

[7] Kuwabara, T. Advances in experiments on metal sheets and tubes in support of constitutive modeling and forming simulations. *Int. J. Plast.* (2007) **23**:385-419.

[8] Brünig, M., Brenner, D. and Gerke, S. Stress state dependence of ductile damage and fracture behavior: Experiments and numerical simulations. *Eng. Fract. Mech.* (2015) **141**:152-169.

[9] Brünig, M., Gerke, S. and Schmidt, M. Biaxial experiments and phenomenological modeling of stress-state-dependent ductile damage and fracture. *Int. J. Fract.* (2016) **200**:63-76.

[10] Gerke, S., Adulyasak, P. and Brünig, M. New biaxially loaded specimens for the analysis of damage and fracture in sheet metals. *Int. J. Solids Struct.* (2017) **110**:209-218.

[11] Gerke, S., Zistl, M., Bhardwaj, A. and Brünig, M. Experiments with the X0-specimen on the effect of non-proportional loading paths on damage and fracture mechanisms in aluminum alloys. *Int. J. Solids Struct.* (2019) **163**:157-169.

[12] Brünig, M. An anisotropic ductile damage model based on irreversible thermodynamics. *Int. J. Plast.* (2003) **19**:1679-1713.

[13] Chow, C. and Wang, J. An anisotropic theory of continuum damage mechanics for ductile fracture. *Eng. Fract. Mech.* (1987) **27**:547-558.

[14] Brünig, M., Gerke, S. and Hagenbrock, V. Micro-mechanical studies on the effect of the stress triaxiality and the Lode parameter on ductile damage. *Int. J. Plast.* (2013) **50**:49-65.

[15] Brünig, M., Gerke, S. Simulation of damage evolution in ductile metals undergoing dynamic loading conditions. *Int. J. Plast.* (2011) **27**:1598-1617.